Impact behaviour of flax/epoxy composite plates

Shaoxiong Liang [a, *], Laurent Guillaumat [a], Papa-Birame Gning [b]

[a] LAMPA, Arts et Métiers ParisTech, 49100 Angers, France
[b] DRIVE–ISAT, Université de Bourgogne, 58027 Nevers, France

A B S T R A C T

This paper presents an experimental investigation of the impact behaviour of flax/epoxy composite plates submitted to low-velocity transverse impact. Low energy drop-weight impact tests have been performed on two types of quasi-isotropic flax/epoxy composites, rectangularly shaped with edges lengths of 142 mm × 94 mm and 2.85 mm thick. Residual properties have been assessed by compression after impact tests. A detailed description of damage development, especially the increase of the rear face crack with respect to the impact energy is given by the microscopic observation. The influence of impact damage on the residual strength is described. A loss of 15%–30% in compression resistance was noticed for specimens impacted by 10 J. Dynamic effects appeared negligible and a good concordance was found between quasi-static three points bending and low energy impact loadings.

1. Introduction

Synthetic fibres reinforced composite materials have been widely used for structural applications due to the weight reduction made possible by their high specific mechanical properties. In the past decade, bio-sourced materials reinforced with vegetal fibres, such as flax, hemp, jute and sisal have gained popularity due to sustainable development requirements and cost-effectiveness [1,2]. Yan et al. [2] suggested that, when considering mechanical performance, cost and yield, flax, hemp and jute are the most promising bio-fibres that can be used instead of glass fibres in composite materials. Recent studies [3–5] have also confirmed the high potential of vegetal fibre reinforced composites (VFRC) as suitable materials for engineering applications due to their significant mechanical properties. However, it is known that improvements of the intrinsic fibre properties, fibre/matrix interfacial bonding and the long-term behaviour in environmental conditions can increase confidence in the use of VFRC. Regarding the mechanical performances of VFRC, only a few studies can be found about impact behaviour [6–9].

Rectangular thin plates are generally described as flat surfaces having a shortest edge to thickness ratio higher than 10. Their analysis requires in-plane and through-thickness properties as well as boundary conditions for the specimen stiffness. Under impact loading, thin plates tend to bend, while thicker plates are likely to undergo compression failure before bending.

The accidental impact at low velocity on flat or cylindrical structures, possibly due to tool drop, hailstone strike, runway debris, etc., has been studied for their possible damage inducing in composites, and the evolution of these damages during fatigue loading. Even with low incident energy, considerable through-thickness damage, while invisible to the naked eye can be created, causing significant reduction of strength, durability and stability of the structure [10,11]. Therefore numerous studies have been performed on that topic for conventional composite structures. Guillaumat et al. [12,13] developed an experimental design methodology to study the influence of testing parameters on impact response. Authors concluded that the consideration of the coupling effect of the mass-velocity of the impactor was more relevant than the incident energy alone.

Some authors have studied the impact behaviour of VFRC, in particular with flax reinforcement. These materials offer comparable quasi-static specific mechanical properties similar to those of glass fibre [4]. Bledzki et al. [6] have investigated the influence of fibre content and void fraction on the low velocity impact response of 2 mm thick flax/epoxy composite plates. The study showed an increase in the damage threshold, maximum contact force and stiffness with the fibre content, while the lost energy and the maximum deflection decreased. Rodriguez et al. [7] presented a comparative study of the impact response of different natural fibres

* Corresponding author. Tel.: +33 2 41 20 73 59.
E-mail address: shaoxiong.liang@ensam.eu (S. Liang).

and glass fibre reinforced composites with a fibre volume fraction of 30%. Flax fibre based composites exhibited the highest impact energy absorption among natural fibre reinforced composites. This justified the choice of using flax fibre reinforcement in the present study. Siengchin and his co-workers [8,9] have investigated the effect of nanoparticles on the impact response of flax woven composites. The experimental results revealed that the presence of SiO_2 or Al_2O_3 particles in flax/polyethylene or flax/PLA laminates reduces the peak force under impact tests. Authors suggested that the particles have promoted the local crack growth and reduced the ductility. The crashworthiness of flax fibre reinforced composites has been investigated by Yan et al. [14] by quasi-static compression test. Results have shown that the flax/epoxy composite tubes have a specific absorption of 41 J/g, which is higher than that of the stainless steel and aluminium tubes.

It is clear from the literature that residual properties after impact are of prime importance when applying damage tolerance concepts. Therefore, many authors have tried to correlate the residual tension or compression strength with impact energy and damage mechanisms. The Compression After Impact (CAI) test is a proven method to measure the residual properties of impacted composite panels. The objective of this test is to assess the damage tolerance of composite specimens by in-plane compression loading, which may cause local buckling initiated by the impact-induced inter-laminar debonding, leading to the premature collapse of the specimen. Many authors tried to evaluate the influence of impact parameters on the CAI resistance. Among their results, it has been pointed out that parameters such as impactor nose geometry (sharp, hemispherical, flat) [15], stitch quality of layers [16], stacking sequence [17,18] and preload could influence significantly the impact response and thus the CAI results. Sanchez-Saez et al. [17] have shown that plates having Quasi-Isotropic (QI) $[45/0/90]_s$ stacking sequence exhibited less normalized CAI reduction than $[0/90]_{3s}$ and woven laminate specimens. Aktas et al. [18] have also noticed a higher CAI strength in QI $[0/90/45/-45]_s$ glass/epoxy laminates than in cross-ply $[0/90/0/90]_s$ laminates. For this reason, the QI layout is chosen in this study.

All these previous studies tell us that although many authors have worked on the damage development of impacted thin composite plates, the impact response and the residual properties of VFRC have still not been thoroughly investigated. The present paper addresses these problems. First, damage developed at different levels of energy, is described based on microscopic inspection of impacted specimens. From the parameters of the impact responses (contact time, bearing capacity deflection, energy absorption and CAI strength), the influence of specimen orientation is evaluated. Finally, the dynamic effect is revealed by comparing the impact response and the quasi-static bending response.

2. Materials and specimens

The composites examined in this work were reinforced with Hermès flax fibres impregnated with SR 8200/SD 8205 epoxy resin system. The fibres took the form of non-crimp balanced fabric with an areal weight of 235(16) g/m^2. The standard deviations are indicated in brackets. Quasi-Isotropic composite panels having $[0/90/45/-45]_{2s}$ stacking sequence, were fabricated by hand lay-up in a hot press machine at 60 °C under 7 bars for 8 h [3]. This manufacturing process resulted in flat plates with a thickness (e) of 2.85 (0.07) mm. The measured fibre volume content, porosity fraction and density were of 44.0 (1.1)%, 0.72 (0.34)% and 1280 (10) kg/m^3 respectively (ASTM D 3171-11).

According to the Classical Laminates Theory (CLT), the in-plane properties are theoretically identical for quasi-isotropic stacking sequence $[0/90/45/-45]_{2s}$ whatever the sample orientation with respect to the in-plane loading. However, the out-of-plane bending properties vary with the specimen orientation as shown in the polar diagram [19,20] plotted on Fig. 1, with the x axis corresponding to the fibre direction in the outer layer, i.e. 0°. The moduli were computed from the mechanical properties of a flax/epoxy unidirectional composite having similar fibre content (Table 1).

From this plot (Fig. 1), it can be seen that the bending modulus at 0° is 13.06 GPa, which is 19% higher than at 90° of 10.98 GPa. In this study, the samples were subjected to impact and quasi-static bending tests, two sorts of out-of-plane loading. For these tests, the rectangle-shaped specimens, with length and width of 142 and 94 mm, were cut-out from the quasi-isotropic composite plate along 0° and 90° direction. This resulted in specimen plates of $[0/90/45/-45]_{2s}$ and $[90/0/-45/45]_{2s}$ lay-ups along their longer edge. Thereafter they were referred to as QI_0 (Fig. 2a) and QI_90 (Fig. 2b), respectively.

3. Experimental methods

In the analysis of the damage mechanisms in thin composite plates under low velocity and energy impact, degradation will be localized in the vicinity of the contact point. For this reason, the problem can be split in two parts by first looking at the damage induced by the projectile-sample interaction, and second, by examining the influence of the impactor's velocity on damage mechanisms. Two series of tests have therefore been performed for dynamic and quasi-static configurations. Finally, CAI tests were performed in order to investigate the interaction between impact damage and residual resistance.

3.1. Impact test

Since the impact speed of accidentally falling objects is often of only a few m/s, the falling weight impact setup is the most appropriate apparatus to reproduce low energy impacts that may occur in service or during handling. In the present study, the low velocity impact tests were performed using a drop weight machine designed by I2M (Institut de Mécanique et d'Ingénierie de Bordeaux, France) [12]. This machine is equipped with an anti-rebound system to avoid further damage after the first impact. A laser sensor is used to measure the displacement of the impactor. Throughout the tests, post-mortem inspection has shown that no penetration or perforation occurred, hence, the deflection of the specimen was considered equal to the impactor displacement after the initial contact. This means that the indentation of the striker was neglected. A piezoelectric sensor was incorporated in the

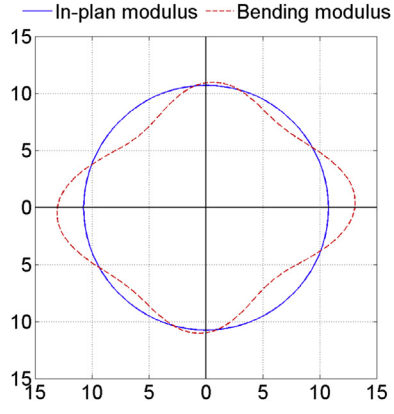

Fig. 1. Polar diagram of membrane and bending moduli of $[0/90/45/-45]_{2s}$ flax/epoxy laminate. The 0° orientation is referred to as the abscissa. Unit in GPa.

Table 1
Elastic properties of a unidirectional flax/epoxy lamina [21]. Standard deviations in brackets.

E_1 (GPa)	E_2 (GPa)	G_{12} (GPa)	ν_{12}
22.8 (1.0)	4.52 (0.18)	1.96 (0.17)	0.43 (0.02)

impactor nose to record the contact force. Data acquisition was sampled at 30 kHz.

The impacts occurred at the centre of the specimens, which was simply supported by two steel supports with a tip diameter of 35 mm. The supports were positioned parallel to the short edge (w) (Fig. 2c) with a span (s) of 100 mm. A high speed CCD (Charge Coupled Device) camera Phantom V4 with a recording rate of 3000 frames/second was used to visualize the impact processes and the films have shown that the specimens were permanently in contact with the supports and the impactor during the test.

The impactor mass (2.044 kg) and geometry (hemispherical, 16 mm in diameter) were constant during all the experiments (Fig. 2c), whereas the nominal impact energy ranged from 2 to 10 J, in 5 equally spaced levels, by setting the drop height appropriately. Two samples were tested for each level for a total of 20 impacted plates.

3.2. Compression after impact (CAI)

Impacted samples were subjected to in-plane compression tests using a CAI device installed on an electromechanical testing machine to measure their residual resistance. The specimens were placed in a jig where the four edges were clamped to prevent global bucking during the compression test (Fig. 3). All tests were performed under constant displacement rate of 1 mm/min. According to the SACMA SRM recommendation [22], the ultimate compressive strength (σ_{UCS}) is calculated by Eq. (1), where P is the ultimate compressive load, w and e are respectively the specimen average width and thickness. Intact specimens have also been tested to get a strength benchmark.

$$\sigma_{UCS} = P/(we) \tag{1}$$

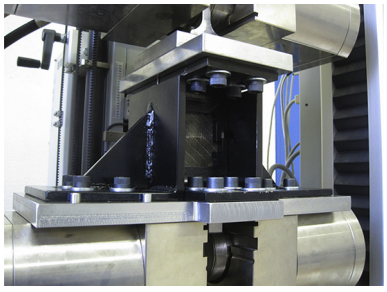

Fig. 3. Compression after impact device.

3.3. Three points bending

Five QI_0 specimens were tested under quasi-static three points bending in order to reproduce the projectile-specimen interaction without any velocity effect. The bending tests were performed using the same geometric conditions as for impact tests (Fig. 2c). These tests were performed on a 100 kN universal testing machine. The moving crosshead was equipped with a hemispherical steel indentor tip of 16 mm of diameter fixed to the machine load cell. The specimens were simply supported by two 35 mm steel cylinders with 100 mm span. The specimens were flexurally loaded up to the average maximum deflection of QI_0 plates during impact tests for each energy level and then unloaded. Tests were conducted under constant displacement speed of 2 mm/min, i.e. 3.33e-5 m/s.

3.4. Damage characterization

The observation of impacted specimens enabled the analysis of the post-mortem damage mechanisms with respect to the impact energy. The specimens were dry cut parallel to the x axis (Fig. 2), by passing through the contact point. Then the samples were moulded in a resin for handling and finely polished polishing with sandpaper and abrasive felts. Surfaces were examined using an Axiovert Optical Microscope.

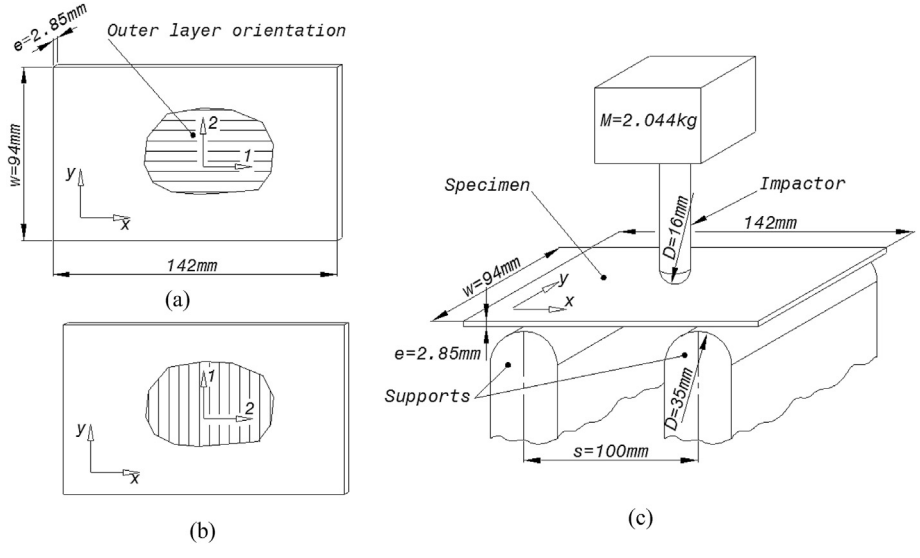

Fig. 2. Schematics of QI_0 (a) and QI_90 (b) specimens: notations with specimen and local coordinates. Impact test setup (c).

4. Results and discussion

4.1. General impact response

The load-time and load-deflexion curves of QI_0 specimens submitted to 2, 6 and 10 J impacts are presented on Fig. 4. 2 J impacts were non-damaging while 6 and 10 J caused visual damage to specimens. The contact force during impact showed significant oscillations. Some authors [10] have suggested that these oscillations are mainly due to the elastic wave responses and the vibration of the specimen. However, the Fast Fourier Transformation of the contact force and the hammer-impact response of the impact device revealed coincidence of the first two eigenmodes at 1.05 and 10.50 kHz. This result implied that the oscillations are mainly caused by the vibrations of the impact system. It is possible to carry out a signal processing using a low pass filter to minimize the oscillations (Fig. 4). The filtered signals plotted in Fig. 4 were obtained with Matlab signal processing function by setting an appropriate cut-off frequency. However, this will also eliminate the vibration of the composite panel. Moreover, the resonance frequency of 1.05 kHz is low and the filtering process can cause boundary smooth error. This error is represented by the "tail" before and after impact process (Fig. 4d–f), implying non-zero force without contact.

As the velocity and impact energy increased, the contact duration and the sample deflection δ also increased as shown on Fig. 4. The area under the loading path of the force–deflection curve (Fig. 4d–f), from δ=0 to δ=δ_{max} represents the impact energy E(Eq. (2)), where $f(\delta)$ is the force as a function of sample deflection. The area under the unloading path after the maximum deflexion, e.g. the integration of the force–deflection curve from δ=δ_{max} to δ=0 is the energy return to the impactor. The difference between the impact energy and the rebound energy is the absorbed energy. It corresponds to the area enclosed between the loading and unloading curves. The energy absorption is due to the damage induced in the specimen and the vibrations of the test device and the striker.

$$E = \int f(\delta) d\delta \tag{2}$$

The contact force as a function of time for QI_0 under 2 J (Fig. 4a) exhibited a half sine wave. In this case, 45% of the impact energy was absorbed by the material. No visible damage was observed on either the impacted or the opposite face of the plate (Fig. 5a).

For a 6 J impact, after the maximum value of 797 N, the force dropped sharply to 566 N. Large amplitude oscillations of the load signal were observed (Fig. 4b and e). This drop is probably due to the creation of a macrocrack, which is visible on the rear face of the specimen (Fig. 5c). On the figure, the filtered signal shows that the force tended to decrease slightly while the deflection continued to increase (Fig. 4b and e) up to the maximum value of 11.21 mm by 7.17 ms. During this process, the macrocrack kept growing up to 32 mm (Fig. 5c). The dissipation processes represented 65% of the incident energy.

The impact-induced macrocrack extended up to the specimen edge (Fig. 5e) for 10 J shock response plotted on Fig. 4c. The load path aspect differed from those at 2 and 6 J. The contact force rose sharply up to a peak value of 892 N at 2.47 ms then dropped to 584 N within 1.29 ms. The macrocrack was assumed to be created at this moment. However, the oscillations induced by the creation of the macrocrack seemed to be not very significant because the amplitude of the oscillations created by the initial contact was still important. The force then tends to be constant while the deflection continues to increase, before another sudden drop of the force, from 720 N to 512 N. This change is supposed to be due to the crack tip reaching the edge of the specimen (Fig. 5). This decreased considerably the stiffness of the specimen. Afterwards, the force seems to reach another plateau of around 550 N until the deflection reaches its maximum value of 15.9 mm before unloading (Fig. 4f). This consideration is confirmed by the fact that for the second 10 J

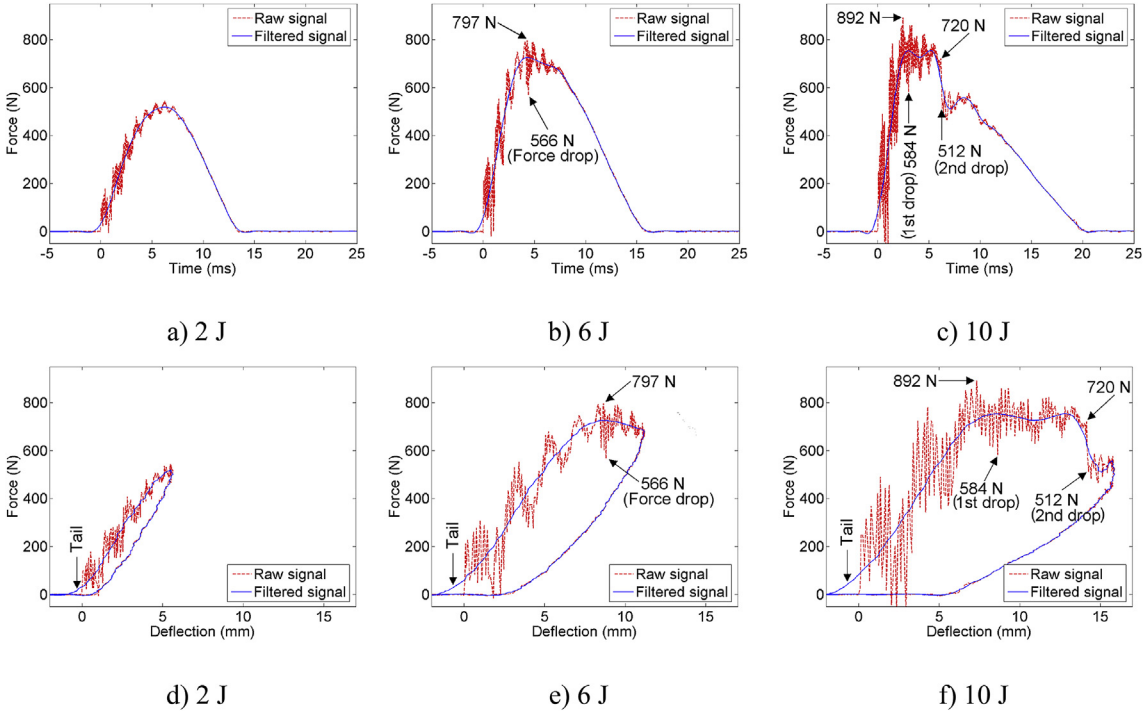

Fig. 4. Load-time history and load-deflection response of QI_0 under 2, 6 and 10 J impact energy.

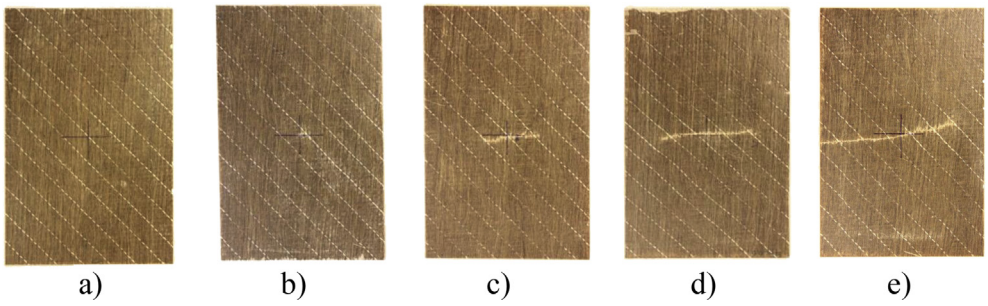

Fig. 5. Rear face view of impacted QI_0 specimens (142 mm × 94 mm) with different energy levels of: a) 2 J, b) 4 J, c) 6 J, d) 8 J, e) 10 J.

sample, for which the crack did not reach the edges, the second drop of load was not observed. 88% of the incident energy was dissipated through the impact.

All of the above remarks can be applied to the QI_90 composite impact tests. It is worth noting that, for this stacking sequence, none of the macrocracks on the two specimens impacted at 10 J has grown up to the edges.

4.2. Damage observation

The post-impact visual inspection did not reveal any damage on the impacted face of QI_0 and QI_90 specimens up to 10 J. A 4 J impact seems to be the minimal energy to initiate a macrocrack, since a suspicious slightly whitened small area, of about 3 mm in diameter, at the centre of the rear face of one of the QI_0 specimens was noticed (Fig. 5b). However, no damage was visible on the 4 J QI_90 impacted samples. For impact energies higher than 4 J, both specimen types showed similar macrocracks of considerable importance on the non-impacted face. One of the 10 J impacted QI_0 plates presents a crack tip going up to the specimen edges (Fig. 5e). The crack propagation did not reach the edges of any QI_90 specimens.

The crack length of QI_0 and QI_90 as a function of the real impact energy (energy evaluated as the area under the force−deflection curves) is plotted on Fig. 6. It is noted that impact energy is, on the average, 17% less than its nominal value due to the friction between the cylinder guides and the impactor. Nevertheless, throughout this work, we refer to the test using their nominal impact energy. Overall, the increase in macrocrack length seems to follow a linear trend with the incident energy above a threshold energy of less than 4 J. The 0° samples presented more severe macro damage than the 90° ones.

Typical microscope images of QI_0 specimens submitted to different impact energy levels are presented on Fig. 7. The subsequent description of the evolution of the damage mechanisms on QI_0 ($[0/90/45/-45]_{2s}$) is based on these images:

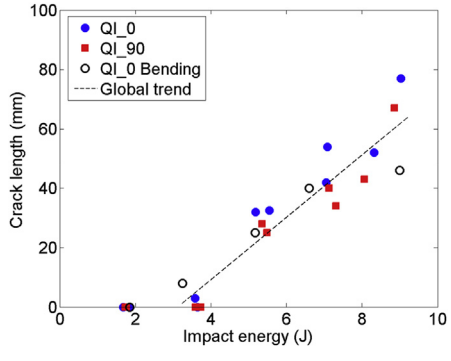

Fig. 6. Crack length on the back of the specimens as a function of incident energy.

- 2 J: Though no visible damage has been observed on the impacted and opposite faces of the specimens (Fig. 5a and Fig. 6), several delaminations (interlaminar debonding) were present in the lower layers (close to the rear face), under the impact point (Fig. 7a).
- 4 J: A significant number of transverse cracks were observed in the lowest 90° layer (Fig. 7b). The intralaminar cracks were similar to those observed in flax/epoxy composites subjected to tensile [21] and fatigue [23] loading. More delamination appeared in the lowest layers than for 2 J impacted specimens.
- 6 J: The breakage of a few fibres belonging to the lowest 0° layer (in the rear face) was observed (Fig. 7c), corresponding to the visible macrocrack on the specimen's rear face (Fig. 5c). The remaining fibres in that layer were distorted, thus forming a local kink-band by compression, probably due to the bouncing process when the composite released the elastic energy back to the impactor during the unloading phase. Delaminations were located between the lower 0/90 layers at the rear face, similar to glass/epoxy composites under impact loading as reported in Ref. [24]. A Complex fracture mechanism combining delamination and transverse cracking has been observed in the lowest quarter of the thickness, near the specimen rear face. It is well known that cracks appear first, and then delamination is induced by the failure of the interface between two layers. Also, a limited number of individual delamination and transverse cracks have propagated in layers close to the front surface. Significant matrix cracks were observed in the resin-rich zones (Fig. 7c). This has not yet been observed in tensile tests before total specimen fracture [21].
- 8 J: Fibres of the lowest 0° layer were broken (Fig. 7d). The second lowest 0° layer was locally distorted during the bouncing back. The complex fracture mechanism combining delamination and transverse cracking extended up to half the thickness. More cracks appeared in layers close to the impacted face, most of them being less than 0.5 mm in length.
- 10 J: A big opening crack in the lower layers was observed (Fig. 7e). Fibres of the lowest 0° layer were fractured, the second lowest 0° layer was distorted and partly broken. Matrix cracking, delamination and interfacial debonding were found in the middle of the thickness. Several cracks in the upper layers reached 0.5−1.5 mm in length.

Overall, the evolution of damage mechanisms in QI_90 samples was similar to that on QI_0. The damage development took place

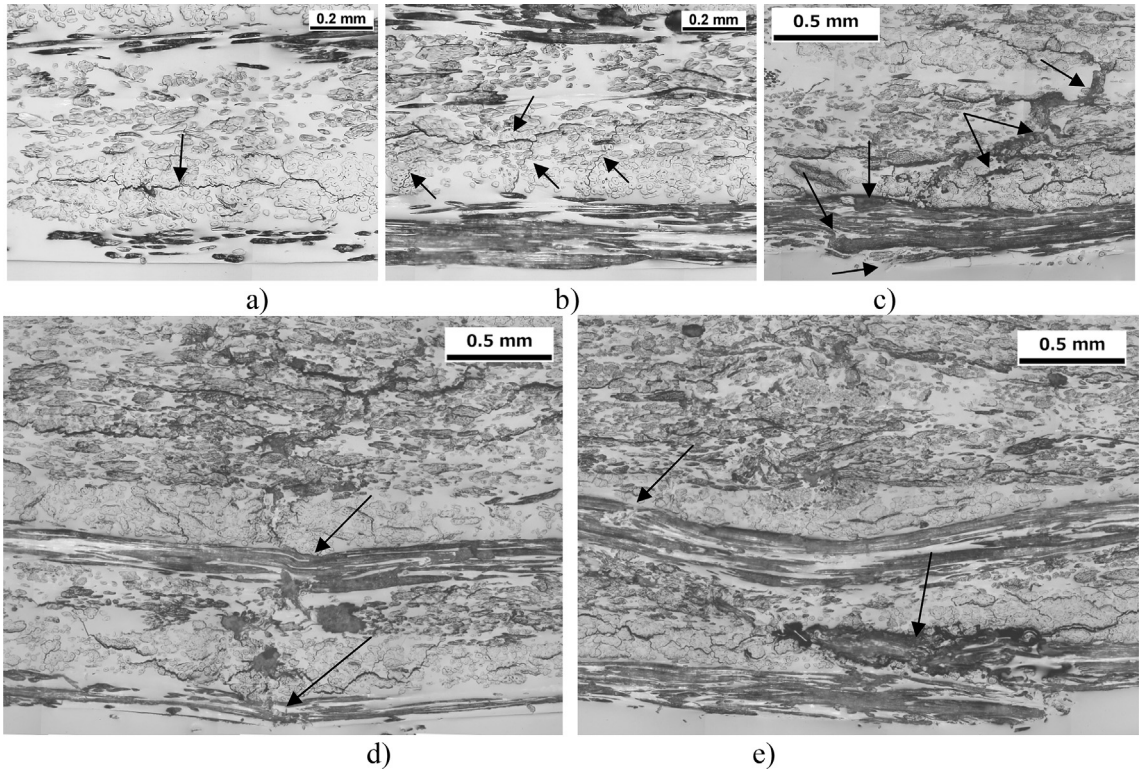

Fig. 7. Damage evolution of impacted QI_0 specimens with different energy levels of: a) 2 J, b) 4 J, c) 6 J, d) 8 J, e) 10 J. Arrows point to the cracks.

first in the lower layers, and then was propagated towards the middle layers with the increase of impact energy. It can be noted that, below 4 J, a number of microcracks have extended to the middle of the sample without visible macrocrack.

4.3. Influence of the stacking sequence

For a better understanding of the difference in impact response of QI_0 and QI_90 composites, the contact duration (contact time), maximum contact force, maximum deflection and absorbed energy as a function of the real incident energy have been plotted on Fig. 8.

Overall, the contact duration increased with the impact energy and remained higher for QI_90 specimens than for QI_0. Schoeppner and Abrate [10] have proposed a relation (Eq. (3)), derived from the simplified one-dimensional mass-spring vibration system, to calculate the load-time history ($F(t)$) of an impact between a heavy projectile and a lightweight sample, for non-damaging (elastic) impact. K represents the bending stiffness of the specimen, M=2.044 kg and V are respectively the projectile mass and the initial impact velocity.

$$F(t) = V\sqrt{KM}\sin\left(\sqrt{Kt/M}\right) \tag{3}$$

The contact duration ($T_{contact}$) is given by Eq. (4) when considering that it is equal to the half period of vibration of the mass-spring system. K is calculated by Eq. (5), where E_b is the specimen bending modulus equal to 13.06 GPa for QI_0 and 10.98 GPa for QI_90 (Fig. 1). I (Eq. (6)) is the moment of inertia with w=94 mm, e=2.85 mm and s=100 mm.

$$T_{contact} = \pi \Big/ \sqrt{K/M} \tag{4}$$

$$K = 48E_bI \Big/ s^3 \tag{5}$$

$$I = we^3 \Big/ 12 \tag{6}$$

The calculated contact durations were of 13.3 ms for QI_0 and 14.5 ms for QI_90 specimens. Compared to the average experimental values of 13.4 ms and 14.3 ms for QI_0 and QI_90, respectively, impacted at 2 J, the predictions were considered very satisfactory. It can be seen from Eq. (4), that the specimen stiffness and the impactor mass are the key parameters influencing the contact duration, whereas the impact velocity has no effect on it. This point is consistent with the experimental results reported in Refs. [25–27] without damage or with only minor damage induced by the impact. As stated previously, the prediction of the load-time curve and the contact duration by Eq. (3) and Eq. (4) is valid only in the case of elastic impact, especially without any damage. Once damage occurs (Figs. 5 and 7), the stiffness of the system decreases, resulting in an increase in contact duration (Fig. 8a). Fig. 8b shows that the maximum deflection increases quite linearly with impact energy and is slightly more important for QI_90 specimens than for QI_0 ones, due to the lower stiffness. Hence, for a given energy, QI_90 needs to deflect more to stock up the same impact energy.

The maximum contact force (Fig. 8c) increases from 2 to 4 J for QI_0 specimens, then remains relatively constant at around 800 N despite the increasing impact energy. For QI_90 samples, the maximum load increases up to an impact energy of 6J, thereafter reaches the same constant value as the QI_0 specimens, despite the scattering at higher energy levels. This plateau of force is usually considered as the specimen load-bearing capacity, therefore, the sudden load drop and the significant force oscillations after this maximum is reached in force-time and load–deflection plots (Fig. 4b and c) are supposed to be related to matrix cracking and

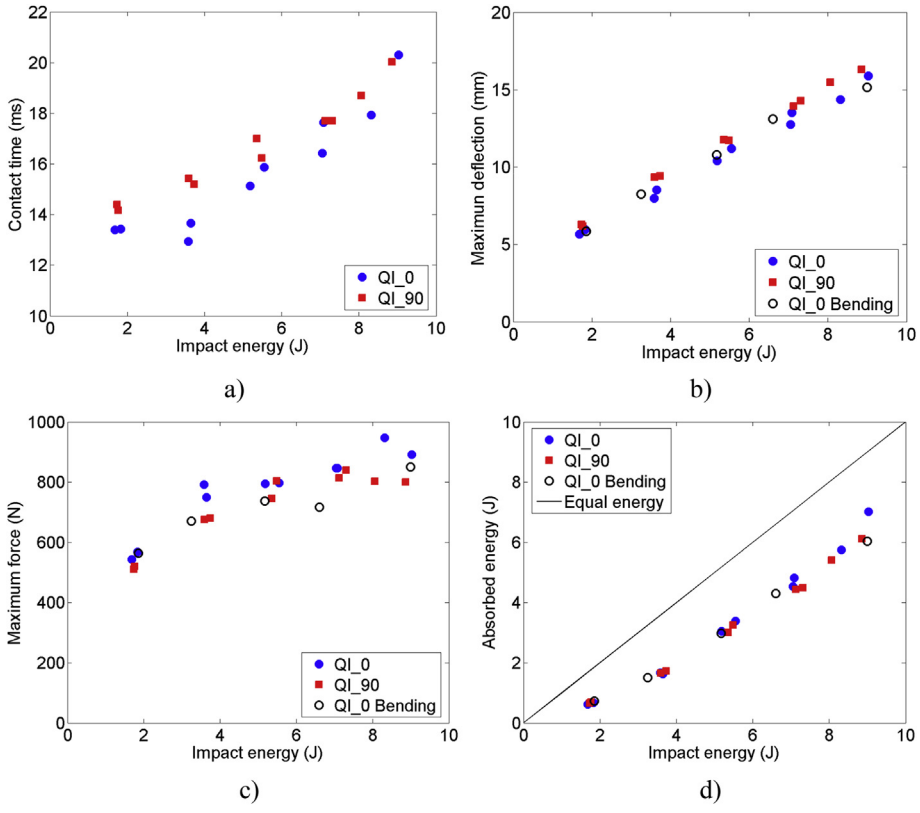

Fig. 8. Evolution of impact response for QI_0 and QI_90 specimens as a function of incident energy: a) contact duration, b) maximum deflection, c) maximum force and d) energy profile.

fibre breakage [25,28]. These damage modes were observed on samples impacted at more than 4 J. Both QI_0 and QI_90 specimen types exhibited the same load-bearing capacity of around 800 N.

The energy profile plotted on Fig. 8d shows a continuous increase of the dissipation with the increase of the incident energy. For a given impact energy level, energy loss is constant for QI_0 and QI_90, in spite of their differences in stiffness. It would be interesting to study higher energy ranges, up to specimen penetration or perforation. However, due to specimen number limitation and duplicated tests to assess the scattering of the results, the consideration of impact tests at a more important energy level is not investigated in this presented study.

4.4. Three points bending

The loading path of QI_0 specimens under impact and quasi-static three points bending test have been compared on Fig. 9. The specimens were deflected to 5.85, 8.25, 10.80, 13.10 and 15.15 mm, corresponding to the average peak deflection for each of the five impact energy levels. As the quasi-static flexion curve to 15.15 mm of deflection did not reveal a second abrupt load drop, its force–deflection curve has been compared to that of the least damaged 10 J impacted plate in Fig. 9e. It can be seen that the quasi-static load curves pass by the middle of those under dynamic loads, which present oscillations due to apparatus and specimen vibrations. This phenomenon reveals that, the flax/epoxy composites did not exhibit significant rate dependency in the explored velocity range.

For quasi-static deflections above 8.25 mm (4 J), the plots present a horizontal plateau at around 750 N, which is less than the peak force of impact tests of around 800 N (Fig. 8c). The surplus of force is due to the additional amplitude of the oscillations in the dynamic response.

In force–deflection curves at impact levels higher than 4 J, the load increases with the deflection while the oscillation amplitude keep on decreasing from the beginning to the maximum force (Fig. 9c–e). Similarly, the quasi-static bending force increases up to a load plateau, concomitantly to the sudden extension of the macrocrack (Fig. 5), which changes both dynamic and static loading paths. As the initiation of the macrocrack creates a local impact, the oscillations in dynamic response are excited again, and results in a sudden increase in oscillation amplitude. The oscillations induced by the macrocrack creation were not observed in quasi-static tests, due to insufficient sampling frequency of 10 Hz. Afterward, the macrocrack continues to grow with further increase in deflection, reducing the stiffness of the sample. Due to the balance between the loss of stiffness and the increase in deflection, the reaction force remains constant for deflections higher than 8.25 mm, however the oscillations in impact signals keep on decreasing during this process.

It can be noted that regarding macrocrack length (Fig. 6), maximum deflection, maximum contact force and absorbed energy (Fig. 8b–d) as a function of the incident energy, as well as the load-deflection curves (Fig. 9), the quasi-static response can be used to predict the low velocity impact response of flax/epoxy composite, in spite of unavoidable statistical scattering.

4.5. CAI strength

The CAI strength of the composites as a function of the incident impact energy has been plotted on Fig. 10. The compression strength trend remains quite constant at up to 6 J of impact energy,

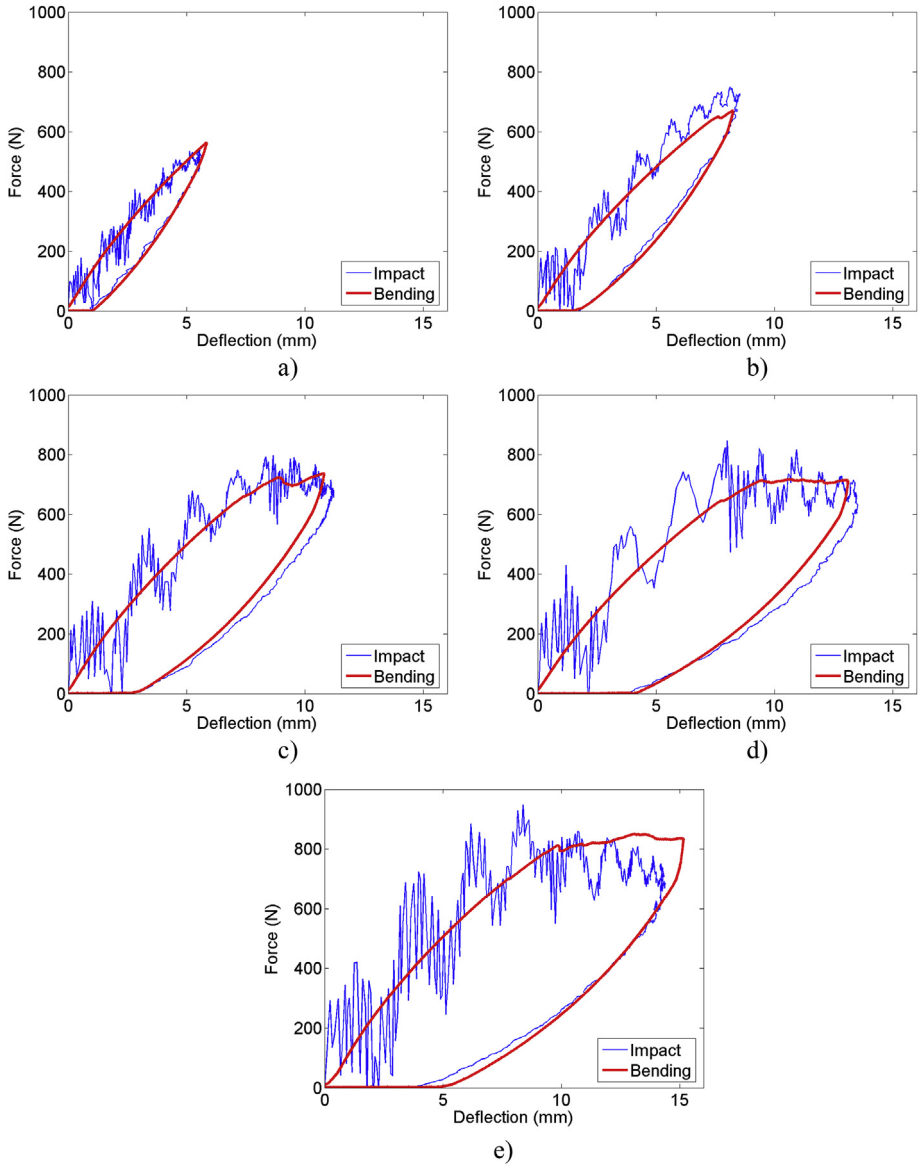

Fig. 9. Comparison of dynamic and corresponding quasi-static loading path of QI_0 specimens under: a) 2 J, b) 4 J, c) 6 J, d) 8 J and e) 10 J.

despite a loss of 2% at that energy for both laminate types. The insignificance of this loss of resistance at 6 J compared to the non-impacted specimens' resistance, can be explained by the non-severity of the pre-existing damage. In fact, only a few fibres of the bottom layer (Fig. 7c) were fractured by the macrocrack (Fig. 5c) and the compression force tended to close the transverse cracks during the CAI loading. The size of the delaminated area was not critical and was confined to a small zone (Fig. 7c). Afterwards, the increase of the impact energy and the damage growth (Fig. 7d and e) resulted in significant CAI strength decrease. The maximum loss was of 30 and 15% for QI_0 and QI_90, respectively, for an impact energy of 10 J. This decrease is comparable to that of glass/epoxy composites (17–34%) reported in Ref. [29].

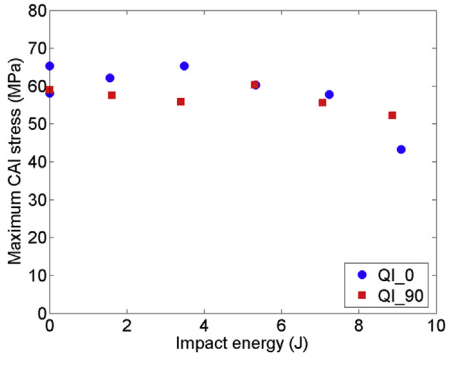

Fig. 10. Evolution of the residual strength as a function of impact energy.

5. Conclusion

Experimental investigations of low velocity impact behaviour of two types of thin quasi-isotropic flax/epoxy composite specimens, i.e. [0/90/45/-45]2s and [90/0/-45/45]2s (QI_0 and QI_90), have been conducted by drop-weight impact, quasi-static three point bending and compression after impact tests.

As can be found for conventional composites, contact time is controlled by the stiffness of the impacted structure and the

impactor mass. The lower bending stiffness of QI_90 specimens resulted in more important impact duration and deflection compared to QI_0 samples. The increase in contact time with the impact energy is due to damage growth. The maximum deflection and the absorbed energy increases with impact energy, without specimen perforation. The peak contact force presents a plateau at around 800 N for impact energies higher than 4 J. The comparison of force–deflection curves, rear face macrocrack length, peak deflection, maximum contact load and absorbed energy shows that flax/epoxy composites do not present significant rate dependence between 3.33e-5 m/s and 2.98 m/s. This confirmed that the impact response of flax/epoxy composites could be satisfactorily predicted by the quasi-static response with consideration of additional oscillations of the impact system. The residual compressive strength dropped by 30% and 15% for QI_0 and for QI_90 specimens impacted at 10 J.

Microscope observation revealed that the crack damage started to take place in the layers in the vicinity of the non-impacted face, then extended towards the interior layers with the increase of impact energy. The fracture mechanism consisted in delaminations that occurred at low energy level, followed by the development of intra-laminar transverse cracks and a macrocrack due to the failure of the fibres of the plate's rear face layer for impact energies above 4 J.

Acknowledgements

Authors thank Angers Loire et Métropole for financing this research. M. Jean-Luc Barou from I2M laboratory is kindly acknowledged for his technical support.

References

[1] Summerscales J, Dissanayake NPJ, Virk AS, Hall W. A review of bast fibres and their composites. Part 1 – fibres as reinforcements. Compos Part A 2010;41:1329–35.
[2] Yan L, Chouw N, Jayaraman K. Flax fibre and its composites – a review. Compos Part B 2014;56:296–317.
[3] Liang S, Gning PB, Guillaumat L. A comparative study of fatigue behaviour of flax/epoxy and glass/epoxy composites. Compos Sci Technol 2012;72(5):535–43.
[4] Wambua P, Ivens J, Verpoest I. Natural fibres: can they replace glass in fibre reinforced plastics? Compos Sci Technol 2003;63(9):1259–64.
[5] Gning PB, Liang S, Guillaumat L, Pui WJ. Influence of process and test parameters on the mechanical properties of flax/epoxy composites using response surface methodology. J Mater Sci 2011;46:6801–11.
[6] Bledzki AK, Gassan J, Zhang W. Impact properties of natural fiber-reinforced epoxy foams. J Cell Plast 1999;35:550–62.
[7] Rodriguez E, Petrucci R, Puglia D, Kenny JM, Zquez AV. Characterization of composites based on natural and glass fibers obtained by vacuum infusion. J Compos Mater 2005;39:265–83.
[8] Siengchin S. Impact, thermal and mechanical properties of high density polyethylene/flax/SiO_2 composites: effect of flax reinforcing structures. J Reinf Plast Compos 2012;31:959–66.
[9] Siengchin S, Pohl T, Medina L, Mitschang P. Structure and properties of flax/polylactide/alumina nanocomposites. J Reinf Plast Compos 2013;32:23–33.
[10] Schoeppner GA, Abrate S. Delamination threshold loads for low velocity impact on composite laminates. Compos Part A 2000;31:903–15.
[11] Gning PB, Tarfaoui M, Collombet F, Riou L, Davies P. Damage development in thick composite tubes under impact loading and influence on implosion pressure: experimental observations. Compos Part B-Engineering 2005;36:306–18.
[12] Guillaumat L, Baudou F, Gomes de Azevedo AM, Lataillade JL. Contribution of the experimental designs for a probabilistic dimensioning of impacted composites. Int J Impact Eng 2005;31:629–41.
[13] Guillaumat L. Reliability of composite structures - impact loading. Comput Struct 2000;76:163–72.
[14] Yan L, Chouw N. Crashworthiness characteristics of flax fibre reinforced epoxy tubes for energy absorption application. Mater Des 2013;51:629–40.
[15] Mitrevski T, Marshall IH, Thomson R. The influence of impactor shape on the damage to composite laminates. Compos Struct 2006;76(1–2):116–22.
[16] Tan KT, Watanabe N, Iwahori Y, Ishikawa T. Effect of stitch density and stitch thread thickness on compression after impact strength and response of stitched composites. Compos Sci Technol 2012;72:587–98.
[17] Sanchez-Saez S, Barbero E, Zaera R, Navarro C. Compression after impact of thin composite laminates. Compos Sci Technol 2005;65:1911–9.
[18] Aktas Mehmet, Ramazan Karakuzu, Yusuf Arman. Compression-after impact behavior of laminated composite plates subjected to low velocity impact in high temperatures. Compos Struct 2009;89:77–82.
[19] Vanucci P, Verchery G. Stiffness design of laminates using the polar method. Int J Solids Struct 2001;38:9281–94.
[20] Vanucci P, Verchery G. A new method for generating fully isotropic laminates. Compos Struct 2002;58:75–82.
[21] Liang S, Gning PB, Guillaumat L. Quasi-static behaviour and damage assessment of flax/epoxy composites. Mater Des 2015;67:344–53.
[22] SACMA SRM 2R–94. Recommended test method for compression after impact properties of oriented fiber–resin composites. Arlington (VA): Suppliers of Advanced Composite Materials Association.
[23] Liang S, Gning PB, Guillaumat L. Properties evolution of flax/epoxy composites under fatigue loading. Int J Fatigue 2014;63:36–45.
[24] Aktas M, Atas C, Icten BM, Karakuzu R. An experimental investigation of the impact response of composite laminates. Compos Struct 2009;87:307–13.
[25] Karakuzu R, Erbil E, Aktas M. Impact characterization of glass/epoxy composite plates: an experimental and numerical study. Compos Part B 2010;41:388–95.
[26] Aktas A, Aktas M, Turan F. The effect of stacking sequence on the impact and post-impact behavior of woven/knit fabric glass/epoxy hybrid composites. Compos Struct 2013;103:119–35.
[27] Icten BM, Atas C, Aktas M, Karakuzu R. Low temperature effect on impact response of quasi-isotropic glass/epoxy laminated plates. Compos Struct 2009;91:318–23.
[28] Caprino G, Lopresto V, Scarponi C, Briotti G. Influence of material thickness on the response of carbon-fabric/epoxy panels to low velocity impact. Compos Sci Technol 1999;59:2279–86.
[29] Icten BM, Kiral BG, Deniz ME. Impactor diameter effect on low velocity impact response of woven glass epoxy composite plates. Compos Part B 2013;50:325–32.